Inorganic Chemistry
Article

Inorg. Chem. **2010**, *49*, 5737–5747 **5737**
DOI: 10.1021/ic100687v

Density Functional Study of the Thermodynamics of Hydrogen Production by Tetrairon Hexathiolate, $Fe_4[MeC(CH_2S)_3]_2(CO)_8$, a Hydrogenase Model

Panida Surawatanawong and Michael B. Hall*

Department of Chemistry, Texas A&M University, College Station, Texas 77843-3255

Received April 11, 2010

The tetranuclear iron complex $Fe_4[MeC(CH_2S)_3]_2(CO)_8$ (**1**) functions like a hydrogenase to catalyze proton reduction to H_2 in the presence of 2,6-dimethylpyridinium acid ($LutH^+$). Experimentally, at the first reduction potential (−1.22 V vs Fc/Fc^+), the concentration of $LutH^+$ decreases slowly, while at the second reduction potential, which is sufficient to reduce $\mathbf{1}^-$ (−1.58 V vs Fc/Fc^+), the concentration of $LutH^+$ decreases more rapidly. Here, density functional theory predicts both reduction potentials (E^0) and proton-transfer free energies relative to $LutH^+$ for numerous intermediates and several important transition states as a basis for developing thermodynamics cycles for routes to hydrogen production by **1**. At the less negative potential, one-electron reduction of **1** is followed by protonation to form a bridging hydride complex; then, a second one-electron reduction is followed by a second protonation, an ECEC process. This doubly reduced and doubly protonated species has a structure with bridging hydrides between both outer Fe−Fe pairs and can produce H_2 and regenerate **1** only by bringing the two hydrogens into proximity through a high-energy intermediate or transition state, a result consistent with the experimentally slow uptake of $LutH^+$ at this potential. In contrast, at the more negative (lower) reduction potential the two-electron-reduced species, $\mathbf{1}^{2-}$, which has bridging carbonyls between both Fe−Fe pairs, is protonated at a terminal Fe position to form a species that produces H_2 by rapidly picking up a second proton and regenerating **1** in an EECC process. Thus, the latter route avoids the high-energy intermediates and transition states necessarily accessed by the former route, a result that explains the more rapid uptake of $LutH^+$ at the second more negative potential. Although both routes arrive at a doubly reduced, singly protonated species in the third step of these processes, the calculations predict that a high barrier prevents the rapid interconversion of these two nearly isoenergetic species. The calculations confirm the importance of terminal metal hydrides, rather than bridging hydrides, for rapid H_2 production and show in detail how the bridging CO maintains the terminal hydride structure at the lower reduction potential even though the bridging hydride conformation is more stable. These results provide clues for designing new biomimic electrocatalysts and further evidence for the terminal Fe−H mechanism in [FeFe]-hydrogenase. The calculations also predict that at even lower reduction potentials, new more highly reduced intermediate species can be accessed that could lead to alternative routes to H_2.

Introduction

Di-iron hydrogenases catalyze the reduction of protons to H_2. X-ray crystal structures reveal that the enzyme's active site, the H-cluster, consists of a di-iron [2Fe] cluster bridged to a [4Fe-4S] cluster by a cysteine ligand from the protein backbone, as shown in Figure 1a.[1,2] Two catalytically active redox states of the di-iron cluster were examined crystallographically: the Fe^IFe^{II} form ($\mathbf{H_{ox}}$)[1] with one CO ligand bridging between the two irons and a weakly bound H_2O on Fe_d, and the Fe^IFe^I form ($\mathbf{H_{red}}$)[2] with the bridging CO in a semibridging position.[2−5] More highly oxidized $Fe^{II}Fe^{II}$ forms are also known but are believed to be catalytically inactive.[6,7]

The design of biomimetic catalysts to simulate the function of hydrogenase is being persued[8−14] both to study the

*To whom correspondence should be addressed. E-mail: mbhall@tamu.edu.

(1) Peters, J. W.; Lanzilotta, W. N.; Lemon, B. J.; Seefeldt, L. C. *Science* **1998**, *282*, 1853–1858.
(2) Nicolet, Y.; de Lacey, A. L.; Vernède, X.; Fernandez, V. M.; Hatchikian, E. C.; Fontecilla-Camps, J. C. *J. Am. Chem. Soc.* **2001**, *123*, 1596–1601.
(3) De Lacey, A. L.; Fernández, V. M.; Rousset, M.; Cammack, R. *Chem. Rev.* **2007**, *107*, 4304–4330.
(4) Siegbahn, P. E. M.; Tye, J. W.; Hall, M. B. *Chem. Rev.* **2007**, *107*, 4414–4435.
(5) Lubitz, W.; Reijerse, E.; van Gastel, M. *Chem. Rev.* **2007**, *107*, 4331–4365.
(6) Pereira, A. S.; Tavares, P.; Moura, I.; Moura, J. J. G.; Huynh, B. H. *J. Am. Chem. Soc.* **2001**, *123*, 2771–2782.
(7) Popescu, C. V.; Münck, E. *J. Am. Chem. Soc.* **1999**, *121*, 7877–7884.
(8) Capon, J.-F.; Gloaguen, F.; Schollhammer, P.; Talarmin, J. *Coord. Chem. Rev.* **2005**, *249*, 1664–1676.
(9) Liu, X.; Ibrahim, S. K.; Tard, C.; Pickett, C. J. *Coord. Chem. Rev.* **2005**, *249*, 1641–1652.
(10) Schmidt, M.; Contakes, S. M.; Rauchfuss, T. B. *J. Am. Chem. Soc.* **1999**, *121*, 9736–9737.
(11) Zhao, X.; Georgakaki, I. P.; Miller, M. L.; Yarbrough, J. C.; Darensbourg, M. Y. *J. Am. Chem. Soc.* **2001**, *123*, 9710–9711.
(12) Barton, B. E.; Rauchfuss, T. B. *Inorg. Chem.* **2008**, *47*, 2261–2263.

Published on Web 05/19/2010

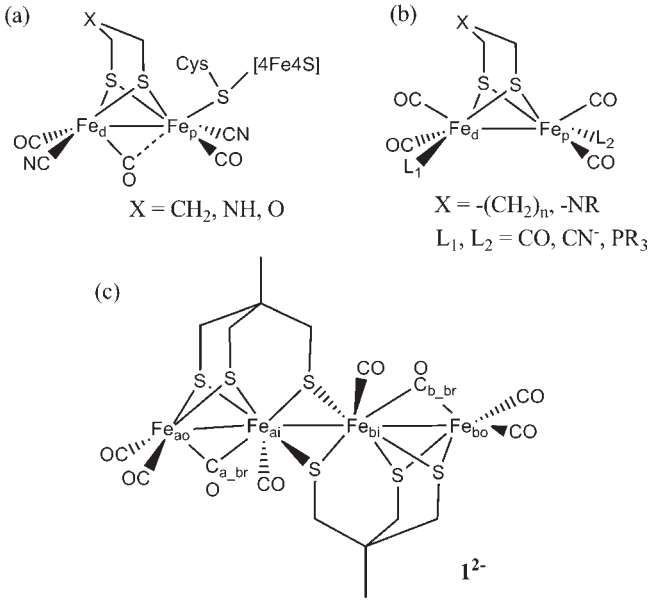

Figure 1. Structures of (a) the di-iron hydrogenase active site, (b) di-iron synthetic models, and (c) $[Fe_4(MeC(CH_2S)_3)_2(CO)_8]^{2-}$ ($\mathbf{1}^{2-}$).

hydrogen production mechanism and as alternative materials for rare and expensive platinum electrodes in hydrogen production and fuel cells.[15−17] Model complexes with structures similar to the active site of hydrogenase, such as di-iron hexacarbonyl dithiolate complexes and their substituted derivatives (Figure 1b), have been studied for hydrogen production reactivity.[8,10−14,18−34] The substitution of CO by better donor ligands, i.e., cyanide,[10] phosphine,[11−13] and cyanide/phosphine,[14] leads to catalysis with weaker acids (higher pH), at less negative reduction potentials, and at higher H_2 production rates. Although the identity of the dithiolate bridgehead in the di-iron hydrogenase structure is unknown, basic sites at the bridging thiolate[29,35] ligands have been introduced in the synthetic model catalysts because of their implications as proton sites. However, the H_2 production rates of these di-iron model complexes are still relatively low compared to di-iron hydrogenases.

There remains a major difference between the stable structures of di-iron model complexes and that of the di-iron subsite in hydrogenases. Although structures of unstable mixed-valence Fe^IFe^{II} model[20,26,36] complexes are found with semi-bridging CO, a structure that resembles the $\mathbf{H_{ox}}$ state of di-iron hydrogenases, stable Fe^IFe^I model complexes have all terminal COs, structures that do not replicate the semibridging CO structure in the $\mathbf{H_{red}}$ state of di-iron hydrogenases. The semibridging carbonyl structure at the [2Fe] subsite in the $\mathbf{H_{red}}$ state of di-iron hydrogenases creates a vacant site on the distal iron (Fe_d), which favors protonation at the terminal position of Fe_d. Furthermore, experimental data on di-iron model complexes show that a terminal hydride can be more active for hydrogen production than a bridging hydride.[24]

Density functional calculations[4] suggest that models of the di-iron hydrogenase active site are protonated either at the Fe−Fe bond for all-terminal CO structures[37,38] or at the terminal position on one Fe for a bridging CO structure.[39−42] De Gioia and co-workers[37] showed that $(\mu\text{-}S(CH_2)_3S)[Fe(CO)_3]_2$ with an all-terminal CO structure leads to hydrogen production between the Fe sites through an intermediate with one hydrogen on each iron. On the other hand, the hydrogen production path through the terminal hydride adducts is more favorable in the density functional calculation of $[(CO)(CN)Fe_d(\mu\text{-DTMA})(\mu\text{-CO})Fe_p(CO)(CN)(SMe)]^-$ (DTMA = SCH_2NHCH_2S) complex,[40,41] in which DTMA can assist the proton-transfer reaction to the terminal site on the distal iron.

More recently, Pickett, Best, and their co-workers synthesized and studied $Fe_4[MeC(CH_2S)_3]_2(CO)_8$ (**1**), a catalyst in which [2Fe3S] units are fused by two bridging thiolate ligands (Figure 1c).[43,44] The catalyst undergoes two one-electron reductions, forming $\mathbf{1}^-$ and $\mathbf{1}^{2-}$ at −1.22 and −1.58 V

(13) Justice, A. K.; Zampella, G.; De Gioia, L.; Rauchfuss, T. B.; van der Vlugt, J. I.; Wilson, S. R. *Inorg. Chem.* **2007**, *46*, 1655–1664.
(14) Gloaguen, F.; Lawrence, J. D.; Rauchfuss, T. B. *J. Am. Chem. Soc.* **2001**, *123*, 9476–9477.
(15) Yaropolov, A. I.; Karyakin, A. A.; Varfolomeev, S. D.; Berezin, I. V. *Bioelectrochem. Bioenerg.* **1984**, *12*, 267–277.
(16) Tye, J. W.; Hall, M. B.; Darensbourg, M. Y. *Proc. Natl. Acad. Sci.* **2005**, *102*, 16911–16912.
(17) Karyakin, A. A.; Morozov, S. V.; Karyakina, E. E.; Varfolomeyev, S. D.; Zorin, N. A.; Cosnier, S. *Electrochem. Commun.* **2002**, *4*, 417–420.
(18) Tye, J. W.; Darensbourg, M. Y.; Hall, M. B. *Inorg. Chem.* **2008**, *47*, 2380–2388.
(19) Tye, J. W.; Lee, J.; Wang, H.-W.; Mejia-Rodriguez, R.; Reibenspies, J. H.; Hall, M. B.; Darensbourg, M. Y. *Inorg. Chem.* **2005**, *44*, 5550–5552.
(20) Liu, T.; Darensbourg, M. Y. *J. Am. Chem. Soc.* **2007**, *129*, 7008–7009.
(21) Thomas, C. M.; Liu, T.; Hall, M. B.; Darensbourg, M. Y. *Inorg. Chem.* **2008**, *47*, 7009.
(22) Tye, J. W.; Darensbourg, M. Y.; Hall, M. B. *Inorg. Chem.* **2006**, *45*, 1552–1559.
(23) Justice, A. K.; Nilges, M. J.; Rauchfuss, T. B.; Wilson, S. R.; De Gioia, L.; Zampella, G. *J. Am. Chem. Soc.* **2008**, *130*, 5293–5301.
(24) van der Vlugt, J. I.; Rauchfuss, T. B.; Whaley, C. M.; Wilson, S. R. *J. Am. Chem. Soc.* **2005**, *127*, 16012–16013. Ezzaher, S.; Capon, J.-F.; Gloaguen, F.; Pétillon, F. Y.; Schollhammer, P.; Talarmin, J.; Pichon, R.; Kervarec, N. *Inorg. Chem.* **2007**, *46*, 3426–3428.
(25) Olsen, M. T.; Bruschi, M.; De Gioia, L.; Rauchfuss, T. B.; Wilson, S. R. *J. Am. Chem. Soc.* **2008**, *130*, 12021–12030.
(26) Justice, A. K.; Rauchfuss, T. B.; Wilson, S. R. *Angew. Chem., Int. Ed.* **2007**, *46*, 6152–6154.
(27) Chong, D.; Georgakaki, I. P.; Mejia-Rodriguez, R.; Sanabria-Chinchilla, J.; Soriaga, M. P.; Darensbourg, M. Y. *Dalton Trans.* **2003**, 4158–4163.
(28) Boyke, C. A.; van der Vlugt, J. I.; Rauchfuss, T. B.; Wilson, S. R.; Zampella, G.; De Gioia, L. *J. Am. Chem. Soc.* **2005**, *127*, 11010–11018.
(29) Capon, J.-F.; Ezzaher, S.; Gloaguen, F.; Pétillon, François Y.; Schollhammer, P.; Talarmin, J. *Chem.—Eur. J.* **2008**, *14*, 1954–1964.
(30) Ezzaher, S.; Capon, J.-F.; Gloaguen, F.; Pétillon, F. Y.; Schollhammer, P.; Talarmin, J. *Inorg. Chem.* **2007**, *46*, 9863–9872.
(31) Song, L.-C.; Wang, L.-X.; Yin, B.-S.; Li, Y.-L.; Zhang, X.-G.; Zhang, Y.-W.; Luo, X.; Hu, Q.-M. *Eur. J. Inorg. Chem.* **2008**, 291–297.
(32) Cheah, M. H.; Borg, S. J.; Bondin, M. I.; Best, S. P. *Inorg. Chem.* **2004**, *43*, 5635–5644.
(33) Cheah, M. H.; Borg, S. J.; Best, S. P. *Inorg. Chem.* **2007**, *46*, 1741–1750.
(34) Borg, S. J.; Behrsing, T.; Best, S. P.; Razavet, M.; Liu, X.; Pickett, C. J. *J. Am. Chem. Soc.* **2004**, *126*, 16988–16999.
(35) Song, L.-C.; Wang, H.-T.; Ge, J.-H.; Mei, S.-Z.; Gao, J.; Wang, L.-X.; Gai, B.; Zhao, L.-Q.; Yan, J.; Wang, Y.-Z. *Organometallics* **2008**, *27*, 1409–1416.
(36) Thomas, C. M.; Darensbourg, M. Y.; Hall, M. B. *J. Inorg. Biochem.* **2007**, *101*, 1752–1757.
(37) Greco, C.; Zampella, G.; Bertini, L.; Bruschi, M.; Fantucci, P.; De Gioia, L. *Inorg. Chem.* **2007**, *46*, 108–116.
(38) Zhou, T.; Mo, Y.; Zhou, Z.; Tsai, K. *Inorg. Chem.* **2005**, *44*, 4941–4946.
(39) Cao, Z.; Hall, M. B. *J. Am. Chem. Soc.* **2001**, *123*, 3734–3742.
(40) Fan, H.-J.; Hall, M. B. *J. Am. Chem. Soc.* **2001**, *123*, 3828–3829.
(41) Zampella, G.; Greco, C.; Fantucci, P.; De Gioia, L. *Inorg. Chem.* **2006**, *45*, 4109–4118.
(42) Liu, Z.-P.; Hu, P. *J. Am. Chem. Soc.* **2002**, *124*, 5175–5182.
(43) Tard, C.; Liu, X.; Hughes, D. L.; Pickett, C. J. *Chem. Commun.* **2005**, 133–135.
(44) Cheah, M. H.; Tard, C.; Borg, S. J.; Liu, X.; Ibrahim, S. K.; Pickett, C. J.; Best, S. P. *J. Am. Chem. Soc.* **2007**, *129*, 11085–11092.

(vs Fc/Fc^+), respectively, in CH_2Cl_2 solvent. The DFT-calculated structures and IR spectra of **1**, $\mathbf{1}^-$, and $\mathbf{1}^{2-}$ in comparison to the IR spectra from spectroelectrochemical (SEC) experiments showed that **1** and $\mathbf{1}^-$ have all-terminal COs structures, whereas $\mathbf{1}^{2-}$ has a bridging CO on each iron pair. Interestingly, unlike other Fe^IFe^I models, which like **1** have all terminal COs,[10−14] the $\mathbf{1}^{2-}$ species with equivalent oxidation states of $4Fe^I$ has a bridging CO structure similar to the structure of the di-iron subsite in the $\mathbf{H_{red}}$ state of di-iron hydrogenase. Moreover, when the 2,6-dimethylpyridinium acid ($LutH^+$) is used as a proton source, the rate of H_2 production for **1** at the lower potential is significantly higher than that for $Fe_2(\mu\text{-}S(CH_2)_3S)(CO)_6$ and $Fe_2(\mu\text{-}PPh(CH_2)_3\text{-}PPh)(CO)_6$.[44] Simulations of the electrochemical results suggested that the slow H_2 production at the first reduction potential is an ECEC process, while the more rapid H_2 production at the second reduction potential is an EECC process.

In this study, we investigated the structure and stability of over 58 possible intermediates involved in proton- and electron-transfer in the H_2 production by **1**. The reduction potentials (E^0) and the proton-transfer free energies relative to $LutH^+$ of these intermediates are calculated and compared to the applied reduction potentials and acidity of $LutH^+$. These density functional studies reveal the most probable intermediates and the key transition states involved in the H_2 production mechanism of the tetra-iron hexa-sulfur catalyst **1** and offer insight into the higher reactivity of $\mathbf{1}^{2-}$ for H_2 production.

Computational Details

All calculations were performed with the Gaussian03 program.[45] The TPSS[46] density functional was used for all geometry optimization and frequency calculation. The Stuttgart RSC 1997 ECP basis set[47] is used for Fe; LANL2DZdp[48] with effective core potential (ECP) is used for sulfur; 6-31G(d,p)[49−51] is used for C, O, and Fe-bound H; and 6-31G(d)[49−51] is used for other hydrogen atoms. A wide range of possible structures was examined, some alternative starting geometries converged to the same structure, and others converged to very high energy structures. Only the lower energy structures are reported here; all were fully optimized with default convergence criteria, and frequencies were calculated to ensure that there are no imaginary frequencies for minima and only one imaginary frequency for transition states. Zero-point energies and thermodynamic functions were calculated at 298.15 K and 1 atm. The solvation energies were calculated on the geometries from TPSS gas-phase optimizations by using the CPCM[52,53] method with UAKS atomic radii and solvation parameters corresponding to CH_2Cl_2 ($\varepsilon = 8.93$). As described below, DFT calculations in conjunction with appropriate solvation models have been used to determine reduction potentials (E^0)[54−58] and proton dissociation constants (pK_a).[59−65] With appropriate parametrization against closely related molecules, these techniques can yield accuracies of ~3 kcal mol^{-1}, $E^0 \pm 0.15$ V, and $pK_a \pm 2$, on moderately sized organic molecules. Although parametrized techniques are under investigation for mononuclear transition metal systems,[66] the accuracy of the unparameterized values reported here will be less. Although we calculated a number of barriers for internal rearrangements of the various species, we have not calculated the rate of H^+ transfer from $LutH^+$, which is likely to be relatively undissociated, nor have we calculated the rate of electron transfer from the electrode. We have assumed that the electron transfer is fast and that internal rearrangements over low barriers are faster than proton transfer from $LutH^+$. These issues will be described for appropriate situations below.

Reduction Potential (E^0) Calculation. The thermodynamic cycle in Scheme 1 is used for calculation of reduction potential of A, $E^0(A)$. The reduction potential can be derived from $\Delta G^{EA}{}_{sol}$ as in eq 1.

$$E^0(A) = -\Delta G^{EA}{}_{sol}/F; F = \text{Faraday constant} \quad (1)$$

$$\Delta G^{EA}{}_{sol} = \Delta G^{EA}{}_{gas} - \Delta G_{solv}(A) - \Delta G_{solv}(e^-) + \Delta G_{solv}(A^-) \quad (2)$$

The $\Delta G^{EA}{}_{sol}$ can be calculated from eq 2 where $\Delta G^{EA}{}_{gas}$ is the free energy change for the electron addition to A in the gas phase and $\Delta G_{solv}(A)$, $\Delta G_{solv}(e^-)$, and $\Delta G_{solv}(A^-)$ are the solvation free energies of A, e^-, and A^-, respectively. The solvation free energy of e^- cannot be obtained directly from the calculation. However, we can eliminate this value through the calculation of relative reduction potentials with a specific reference redox couple; here, we chose ferrocene/ferrocinium (Fc/Fc^+). The relative

(45) Frisch, M. J.; Trucks, G. W.; Schlegel, H. B.; Scuseria, G. E.; Robb, M. A.; Cheeseman, J. R.; Montgomery, J. A., Jr.; Vreven, T.; Kudin, K. N.; Burant, J. C.; Millam, J. M.; Iyengar, S. S.; Tomasi, J.; Barone, V.; Mennucci, B.; Cossi, M.; Scalmani, G.; Rega, N.; Petersson, G. A.; Nakatsuji, H.; Hada, M.; Ehara, M.; Toyota, K.; Fukuda, R.; Hasegawa, J.; Ishida, M.; Nakajima, T.; Honda, Y.; Kitao, O.; Nakai, H.; Klene, M.; Li, X.; Knox, J. E.; Hratchian, H. P.; Cross, J. B.; Adamo, C.; Jaramillo, J.; Gomperts, R.; Stratmann, R. E.; Yazyev, O.; Austin, A. J.; Cammi, R.; Pomelli, C.; Ochterski, J. W.; Ayala, P. Y.; Morokuma, K.; Voth, G. A.; Salvador, P.; Dannenberg, J. J.; Zakrzewski, V. G.; Dapprich, S.; Daniels, A. D.; Strain, M. C.; Farkas, O.; Malick, D. K.; Rabuck, A. D.; Raghavachari, K.; Foresman, J. B.; Ortiz, J. V.; Cui, Q.; Baboul, A. G.; Clifford, S.; Cioslowski, J.; Stefanov, B. B.; Liu, G.; Liashenko, A.; Piskorz, P.; Komaromi, I.; Martin, R. L.; Fox, D. J.; Keith, T.; Al-Laham, M. A.; Peng, C. Y.; Nanayakkara, A.; Challacombe, M.; Gill, P. M. W.; Johnson, B.; Chen, W.; Wong, M. W.; Gonzalez, C.; Pople, J. A. *Gaussian 03, Revision B.4, B.5, and C.1*; Gaussian, Inc.: Pittsburgh, PA, 2003.
(46) Tao, J.; Perdew, J. P.; Staroverov, V. N.; Scuseria, G. E. *Phys. Rev. Lett.* **2003**, *91*, 146401.
(47) Bergner, A.; Dolg, M.; Kuumlchle, W.; Stoll, H.; Preuszlig, H. *Mol. Phys.* **1993**, *80*, 1431.
(48) Wadt, W. R.; Hay, P. J. *J. Chem. Phys.* **1985**, *82*, 284.
(49) Hariharan, P. C.; Pople, J. A. *Theor. Chim. Acta* **1973**, *28*, 213–222.
(50) Petersson, G. A.; Al-Laham, M. A. *J. Chem. Phys.* **1991**, *94*, 6081–6090.
(51) Petersson, G. A.; Bennett, A.; Tensfeldt, T. G.; Al-Laham, M. A.; Shirley, W. A.; Mantzaris, J. *J. Chem. Phys.* **1988**, *89*, 2193–2218.
(52) Barone, V.; Cossi, M. *J. Phys. Chem. A* **1998**, *102*, 1995.
(53) Cossi, M.; Rega, N.; Scalmani, G.; Barone, V. *J. Comput. Chem.* **2003**, *24*, 669–681.
(54) Patterson, E. V.; Cramer, C. J.; Truhlar, D. G. *J. Am. Chem. Soc.* **2001**, *123*, 2025–2031.
(55) Fu, Y.; Liu, L.; Yu, H.-Z.; Wang, Y.-M.; Guo, Q.-X. *J. Am. Chem. Soc.* **2005**, *127*, 7227–7234.
(56) Holland, J. P.; Green, J. C.; Dilworth, J. R. *Dalton Trans.* **2006**, 783–794.
(57) Jan, M.; Paul, G.; Goedele, R. *Chem.—Eur. J.* **2007**, *13*, 8174–8184.
(58) Pakiari, A. H.; Siahrostami, S.; Mohajeri, A. *THEOCHEM* **2008**, *870*, 10–14.
(59) Gossens, C.; Dorcier, A.; Dyson, P. J.; Rothlisberger, U. *Organometallics* **2007**, *26*, 3969–3975.
(60) Ding, F.; Smith, J. M.; Wang, H. *J. Org. Chem.* **2009**, *74*, 2679–2691.
(61) Charif, I. E.; Mekelleche, S. M.; Villemin, D.; Mora-Diez, N. *THEOCHEM* **2007**, *818*, 1–6.
(62) Bryantsev, V. S.; Diallo, M. S.; Goddard, W. A., III. *J. Phys. Chem. A* **2007**, *111*, 4422–4430.
(63) Jang, Y. H.; Goddard, W. A., III; Noyes, K. T.; Sowers, L. C.; Hwang, S.; Chung, D. S. *Chem. Res. Toxicol.* **2002**, *15*, 1023–1035.
(64) Zhang, J.; Sun, Y.; Mao, C.; Gao, H.; Zhou, W.; Zhou, Z. *THEOCHEM* **2009**, *906*, 46–49.
(65) Liptak, M. D.; Shields, G. C. *J. Am. Chem. Soc.* **2001**, *123*, 7314–7319.
(66) Galstyan, A; Knapp, E.-W. *J. Comput. Chem.* **2009**, *30*, 203–211.

Scheme 1. Thermodynamic Cycle of Electron Reduction

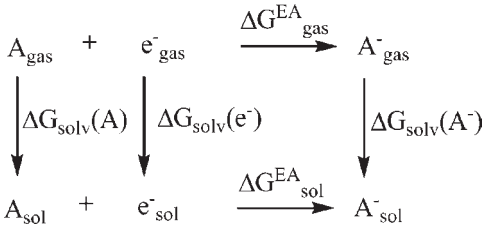

reduction potential of the half reaction $A + e^- \rightarrow A^-$ vs $Fc^+ + e^- \rightarrow Fc$ is reported as shown in eq 3.

$$E^0(\mathrm{A})\ \mathrm{vs}\ (\mathrm{Fc/Fc^+}) = E^0(\mathrm{A}) - E^0(\mathrm{Fc^+}) \quad (3)$$

Our work on di-iron model complexes shows that with the procedure described above [0/1−] E^0's will be calculated too positive, while [1−/2−] E^0's will be calculated too negative.[67]

Proton-Transfer Free Energy Calculation. The Brønsted acidity of a particular compound is usually reported as its proton dissociation constant (pK_a). The thermodynamic cycle in Scheme 2 can be used for the calculation of the free energy change upon proton loss, $\Delta G^{PL}{}_{sol}$ (eq 4), which is related to the pK_a of AH^+ (eq 5).

$$\Delta G^{PL}{}_{sol} = \Delta G^{PL}{}_{gas} + \Delta G_{solv}(\mathrm{A}) + \Delta G_{solv}(\mathrm{H^+}) - \Delta G_{solv}(\mathrm{AH^+}) \quad (4)$$

$$pK_a = \Delta G^{PL}{}_{sol}/2.303RT \quad (5)$$

In eq 4, only the proton solvation free energy, $\Delta G_{solv}(H^+)$, cannot be calculated quantum mechanically. Although, it can be deduced experimentally from the pK_a of a known acid, to the best of our knowledge, neither the proton solvation free energy nor the pK_a of $LutH^+$ in CH_2Cl_2 solvent is known experimentally. Thus, we cannot calculate the pK_a of the intermediate AH^+ by using the known pK_a of $LutH^+$ in CH_2Cl_2. Fortunately, essentially the same information is available by calculating the free energy change to transfer a proton from $LutH^+$ to A (eq 6), and this direct comparison between AH^+ and $LutH^+$ avoids the need to determine the pK_a.

$$\mathrm{A} + \mathrm{LutH^+} \rightarrow \mathrm{AH^+} + \mathrm{Lut} \quad (6)$$

The free energy in CH_2Cl_2 for the reaction in eq 6 will be referred to as proton-transfer free energy to A, and when it is negative, $LutH^+$ is more acidic than AH^+.

Results and Discussion

We investigated the hydrogen production by **1** in the presence of $LutH^+$ by beginning with the calculation of the one- and two-electron-reduced forms of **1** ($\mathbf{1}^-$ and $\mathbf{1}^{2-}$) and following that with calculations of the proton transfers to **1**, $\mathbf{1}^-$, and $\mathbf{1}^{2-}$ to form **H-1**$^+$, **H-1**, and **H-1**$^-$, respectively. We calculated alternative structures for **H-1**^{x} ($x = 1+, 0, 1-$, and 2−) based on the arrangement of the hydride and carbonyl ligands to determine the most stable structure of each species. Although bridging S can be protonated in these species, barriers for H_2 production from such species are large,[39] and we have not considered them further. Various structures of **2H-1**^{x} and **3H-1**^{x} ($x = 1+, 0$, and 1−) from the second and third proton addition were also examined. Then, the proton-transfer free energies of the more stable structures for each species were calculated. The reduction potentials of intermediates relative to ferrocenium (Fc^+) are also calculated to compare with the applied reduction potential. Finally, the overall scheme for hydrogen production is constructed to show the most probable intermediates in the catalytic cycle.

Scheme 2. Thermodynamic Cycle of Proton Dissociation

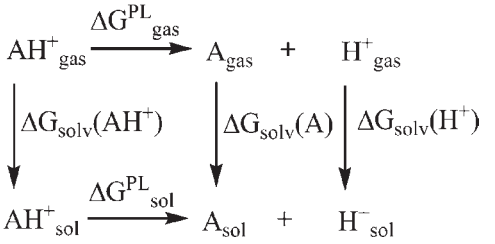

1. Structure Determination of 1, $\mathbf{1}^-$, and $\mathbf{1}^{2-}$. The computed structures of **1**, $\mathbf{1}^-$, and $\mathbf{1}^{2-}$, described briefly below, are in excellent agreement with the experimental structure of **1**, the IR spectra, and structures computed previously with a different functional.[44] The calculated minimum-energy structure of **1** has all terminal COs on both outer Fe atoms with C_i symmetry (Figure 2). The Mulliken atomic charges show that the outer Fe atoms (Fe_{ao} and Fe_{bo}) are more electron rich than the inner Fe atoms (Fe_{ai} and Fe_{bi}) (−0.873 and −0.552, respectively) (Table 1). The formal oxidation numbers of Fe in **1** could be assigned as $Fe^{1+}Fe^{2+}Fe^{2+}Fe^{1+}$; this assignment parallels the Mulliken charges, but one should not expect to find numerical similarity, as the formal charges assign metal−ligand bonding pairs to the ligand, while the Mulliken charge partitions these electrons between the metal and ligand atom (APT charges, see SI, parallel the Mulliken charges). Furthermore, the MOs are very delocalized (see SI), which would suggest that the inner Fe^{2+} are open-shell and antiferromagnetically coupled to the adjacent Fe's. The $Fe_{ao}-Fe_{ai}$ bond is 2.527 Å, whereas the $Fe_{ai}-Fe_{bi}$ bond is slightly longer (2.618 Å) (Figure 2 and Table 2). Experimentally, these bond distances are 2.543 and 2.651 Å,[43] respectively, while the previous DFT calculations gave 2.544 and 2.628 Å,[44] respectively. We also determined a structure with one terminal CO on Fe_{ao} rotated to the semibridging position between $Fe_{ao}-Fe_{ai}$, **1(TS)**, a transition state 9.00 kcal/mol less stable than **1**.

The first electron reduction forms $\mathbf{1}^-$, which has a minimum-energy structure similar to **1**, C_i symmetry, and all terminal COs. The main difference is that the $Fe_{ai}-Fe_{bi}$ bond distance in $\mathbf{1}^-$ lengthens to 2.900 Å, a change that results from the electron occupation of the LUMO of **1** that is $Fe_{ai}-Fe_{bi}$ antibonding (in SI see Figures S1 and S2). The unpaired electron in $\mathbf{1}^-$ is located mainly on inner Fe atoms; spin densities on Fe_{ai} and Fe_{bi} are 0.492, whereas spin densities on outer irons, Fe_{ao} and Fe_{bo}, are 0.023 (Table 3). The charge density rearranges such that the outer Fe's (−0.923) have even more electrons and the inner Fe's (−0.423) have fewer electrons in spite of the added electron residing mainly on the inner Fe's. The oxidation number of Fe could be assigned as $Fe^{1+}Fe^{1.5+}Fe^{1.5+}Fe^{1+}$ or an antiferromagnetically coupled $Fe^{0.5+}Fe^{2+}Fe^{2+}Fe^{0.5+}$. The structure with a single semibridging CO between $Fe_{ao}-Fe_{ai}$, $\mathbf{1(TS)}^-$, is also determined to be a transition state, now only 3.39 kcal/mol less stable than $\mathbf{1}^-$.

The second electron reduction forms $\mathbf{1}^{2-}$. Unlike **1** and $\mathbf{1}^-$, the minimum-energy structure of $\mathbf{1}^{2-}$ has bridging

(67) Surawatanawong, P.; Tye, J. W.; Darensbourg, M. Y.; Hall, M. B. *Dalton Trans.* **2010**, 3093–3104.

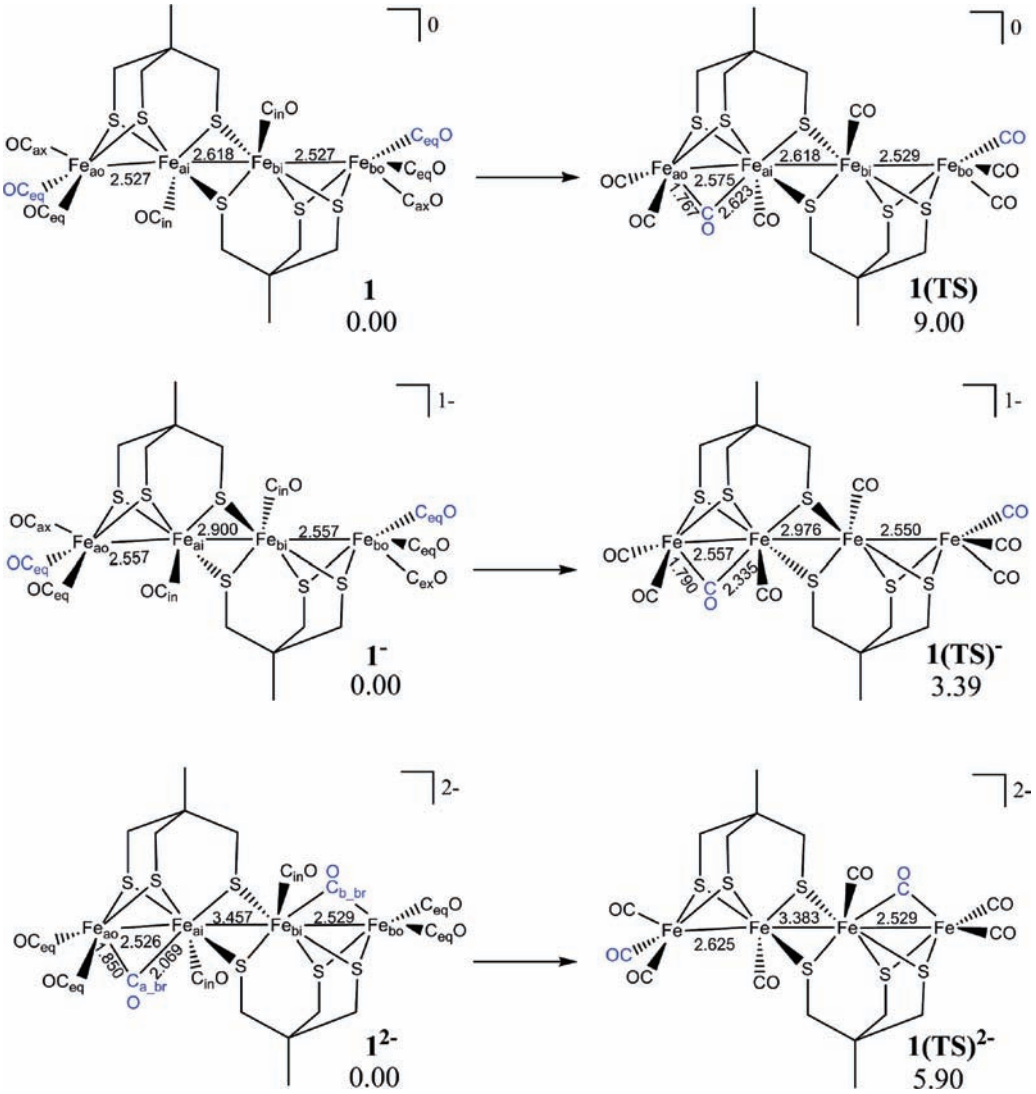

Figure 2. Rotation of carbonyl on one of the irons of **1**, $\mathbf{1}^-$, and $\mathbf{1}^{2-}$. The relative free energies in CH_2Cl_2 solution are given in kcal/mol. Selected bond distances are given in Å.

Table 1. Mulliken Atomic Charges of **nH-1**^{x} (n = 0, 1, 2, and 3; x = 2−, 1−, and 0)

	1	$\mathbf{1}^-$	$\mathbf{1}^{2-}$	**H-1(d)**	**H-1(b)**$^-$	**H-1(c)**$^-$	**H-1(c)**$^{2-}$	**2H-1(d)**	**2H-1(e)**	**2H-1(c)**$^-$	**2H-1(d)**$^-$	**2H-1(e)**$^-$	**3H-1(d)**	**3H-1(c)**$^-$
Fe_{ao}	−0.873	−0.923	−0.587	−0.863	−0.603	−0.862	−0.924	−0.979	−0.993	−0.832	−0.912	−1.033	−0.643	−1.029
Fe_{ai}	−0.552	−0.423	−0.700	−0.432	−0.660	−0.784	−0.752	−0.614	−0.443	−0.778	−0.711	−0.455	−0.718	−0.681
Fe_{bi}	−0.552	−0.423	−0.700	−0.617	−0.667	−0.736	−0.742	−0.677	−0.563	−0.785	−0.696	−0.564	−0.675	−0.738
Fe_{bo}	−0.873	−0.923	−0.587	−1.008	−1.019	−0.570	−0.626	−0.953	−0.929	−0.686	−1.014	−0.975	−0.969	−0.945
C_{a_br}			0.546		0.541	0.550	0.543	0.542		0.535	0.548		0.531	
C_{b_br}			0.546			0.545	0.552			0.559				
H_{a_br}									0.069			0.068		0.126
H_{b_br}				0.143	0.125			0.124	0.067		0.127	0.070	0.121	0.071
H_{ao_t1}						0.117	0.078	0.212		0.078	0.105		0.062	
H_{ao_t2}										0.087			0.066	
H_{bi_t}														0.150
H_{bo_t}														

COs between both $Fe_{ao}-Fe_{ai}$ and $Fe_{bo}-Fe_{bi}$ with the $Fe_{ai}-C_{a\_br}$ bond (2.069 Å) slightly longer than the $Fe_{ao}-C_{a\_br}$ bond (1.850 Å). The $Fe_{ai}-Fe_{bi}$ bond distance in $\mathbf{1}^{2-}$ further extends to 3.457 Å, corresponding to a fully occupied $Fe_{ai}-Fe_{bi}$ antibonding orbital (Figure S3). Now, the atomic charges on the outer Fe atoms (−0.587) are less negative than those on the inner Fe atoms (−0.700) (Table 1). Supported by the arrangement of CO ligands in the bridging CO structure of $\mathbf{1}^{2-}$, the back-bonding from the outer Fe not only to the bridging CO but also to the equatorial COs as shown in HOMO−1 and HOMO−2 orbitals (Figure S3) results in the lengthening of all CO bonds in comparison to **1** and $\mathbf{1}^-$ (Table 2). The oxidation number of Fe atoms could be assigned as a mixture of $Fe^{1+}Fe^{1+}Fe^{1+}Fe^{1+}$ and $Fe^{0}Fe^{2+}Fe^{2+}Fe^{0}$. The MOs (see SI) suggest that substantial Fe 3d lone pair character exists on the outer Fe's. The structure with only one semibridging CO on one of the inner−outer Fe pairs,

Table 2. Selected Geometry Parameters of *n*H-1^x (n = 0, 1, 2, and 3; x = 2−, 1−, and 0)

	1	1$^-$	1^{2-}	H-1(d)	H-1(b)$^-$	H-1(c)$^-$	H-1(c)$^{2-}$	2H-1(d)	2H-1(e)	2H-1(c)$^-$	2H-1(d)$^-$	2H-1(e)$^-$	3H-1(d)	3H-1(c)$^-$
$Fe_{ao}-Fe_{ai}$	2.527	2.557	2.526	2.517	2.525	2.524	2.660	2.502	2.581	2.725	2.591	2.686	2.691	2.606
$Fe_{ai}-Fe_{bi}$	2.618	2.900	3.457	2.934	3.353	3.433	3.517	3.386	3.305	3.456	3.378	3.254	3.403	3.380
$Fe_{bo}-Fe_{bi}$	2.527	2.557	2.529	2.616	2.605	2.518	2.524	2.578	2.580	2.519	2.666	2.686	2.580	3.129
$Fe_{ao}-C_{a\_br}$			1.850		1.822	2.107	2.071	2.033		2.386	2.037		2.258	
$Fe_{ai}-C_{a\_br}$			2.069		2.130	1.898	1.911	1.947		1.821	1.949		1.844	
$Fe_{bi}-C_{b\_br}$			2.071			2.136	2.067			2.120				
$Fe_{bo}-C_{b\_br}$			1.850			1.820	1.851			1.823				
$Fe_{ao}-H_{a\_br}$									1.700			1.735		1.731
$Fe_{ai}-H_{a\_br}$									1.673			1.663		1.660
$Fe_{bi}-H_{b\_br}$				1.703	1.678			1.670	1.673		1.667	1.662	1.672	1.773
$Fe_{bo}-H_{b\_br}$				1.662	1.708			1.702	1.701		1.736	1.736	1.701	2.084
$Fe_{ao}-Ha_{o\_t1}$						1.506	1.548	1.506		1.876	1.529		1.830	
$Fe_{ao}-Ha_{o\_t2}$										1.874			1.835	
$Fe_{bi}-H_{bi\_t}$														1.640
$Fe_{bo}-H_{bo\_t}$														
$H_{ao\_t1}-H_{ao\_t2}$										0.777			0.781	
$H_{bi\_t}-H_{b\_br}$														0.857
$O-C_{a\_br}$			1.194											
$O-c_{ax}$	1.166	1.174												
$O-c_{eq}$	1.164	1.171	1.185											
$O-c_{in}$	1.172	1.178	1.180											
$O-C_{b\_br}$			1.194											

Table 3. Mulliken Spin Densities of *n*H-1^x (n = 0, 1, 2, and 3; x = 2−, 1−, and 0)

	1$^-$	H-1(d)	H-1(c)$^{2-}$	2H-1(c)$^-$	2H-1(d)$^-$	2H-1(e)$^-$	3H-1(d)
Fe_{ao}	0.023	−0.058	0.311	0.754	0.148	0.187	0.849
Fe_{ai}	0.492	0.888	0.500	0.227	0.342	0.175	0.201
Fe_{bi}	0.492	0.230	0.013	0.020	0.220	0.298	0.005
Fe_{bo}	0.023	0.022	−0.001	−0.001	0.273	0.402	0.000
C_{a_br}			0.059	−0.014	0.034		−0.015
C_{b_br}			−0.001	0.000			
H_{a_br}						−0.017	
H_{b_br}		0.001			−0.012	−0.014	0.000
H_{ao_t1}			0.056	0.010	0.028		0.029
H_{ao_t2}				0.045			0.010
H_{bi}							
H_{bo_t}							

1(TS)$^{2-}$, is also determined to be a transition state that is less stable than **1**$^{2-}$ by 5.90 kcal/mol. Note that the all-Fe^{1+} structure of this tetra-iron species displays bridging COs, while the corresponding structures of the all-Fe^{1+} di-iron model compounds show all terminal COs. Interestingly, bridging CO structures are predicted to appear in the di-iron species when the complex is made electron rich enough by strong donors or when the Fe−Fe is weakened by reduction or oxidation.[18] The appearance of CO bridging structures in the all-Fe^{1+} tetra-iron systems is a reflection of the electron-rich character caused by the strong S donor ligands, the fewer COs, and the negative overall charge.

2. First Proton Addition: H-1$^+$, H-1, H-1$^-$, and H-1^{2-}. The possible structures for **H-1**^{x} (x = 2−, 1−, 0, and 1+) based on various hydride and CO ligand arrangements are shown in Figure 3. The addition of the first proton to **1** forms **H-1**$^+$. **H-1(a)**$^+$ and **H-1(c)**$^+$ are less stable than **H-1(d)**$^+$ by 15.01 and 38.58 kcal/mol, respectively (Table 4). **H-1(b)**$^+$ could not be located; instead, the bridging CO rotates to the terminal position, becoming **H-1(d)**$^+$ after geometry optimization. The most stable structure, **H-1(d)**$^+$, has a hydride bridging (H_{b_br}) between $Fe_{bi}-Fe_{bo}$ and all terminal COs on both outer Fe's. The proton-transfer free energy to **1** to form **H-1(d)**$^+$ is unfavorable (relative to $LutH^+$) by 21.46 kcal/mol (Table 5). Therefore, the formation of any **H-1**$^+$ species in the reaction is unlikely because the most stable from, **H-1(d)**$^+$, is much more acidic than $LutH^+$.

The addition of the first proton to **1**$^-$ forms **H-1** (Figure 3). Like the cationic species above, **H-1(a)** and **H-1(c)** are less stable than **H-1(d)** (Table 4). Here, **H-1(b)** was located, but it is still less stable than **H-1(d)** by 10.78 kcal/mol. Unlike the cationic species, the proton-transfer free energy to **1**$^-$ to form **H-1(d)** is favorable by −6.25 kcal/mol (Table 5). Thus, the **H-1(d)** can be formed readily in the electrocatalytic reaction. The atomic charges on outer iron atoms are still more negative than that on inner iron atoms (Table 1); furthermore, the atomic charges on $Fe_{bi}-Fe_{bo}$, the pair with a bridging hydride (H_{b_br}), are more negative than those on $Fe_{ai}-Fe_{ao}$, the pair without the bridging hydride. In comparison to **1**$^-$, the $Fe_{bi}-Fe_{bo}$ bond and the $Fe_{ai}-Fe_{bi}$ bond in **H-1(d)** lengthen by 0.06 and 0.03 Å, respectively, whereas the $Fe_{ai}-Fe_{ao}$ bond shortens by 0.04 Å (Table 2). Mulliken analysis shows that the unpaired electron in **H-1(d)** is located mainly on the inner Fe atoms with some on Fe_{bi} (0.230) and a larger amount on Fe_{ai} (0.888), the atom without the bridging H (Table 3).

The addition of the first proton to **1**$^{2-}$ forms **H-1**$^-$ (Figure 3). Here, structure **H-1(d)**$^-$ is a transition state with an imaginary vibrational mode for CO rotating about the outer iron from a terminal to a bridging position to form **H-1(b)**$^-$; a similar situation is also found for **H-1(a)**$^-$, which transforms to **H-1(c)**$^-$. Since **H-1(a)**$^-$ and **H-1(d)**$^-$ are transition states, they will decay rapidly to **H-1(c)**$^-$ and **H-1(b)**$^-$, respectively, and the rates of these decays should be fast compared to the electron or proton transfer. **H-1(d)**$^-$ and **H-1(a)**$^-$ have higher energies than **H-1(b)**$^-$, the lowest energy structure, by 5.52 and 7.34 kcal/mol, respectively (Table 4). **H-1(c)**$^-$, the structure expected to form initially from protonation of **1**$^{2-}$, with a terminal hydride (H_{ao_t1}) on Fe_{ao} and bridging COs between $Fe_{ai}-Fe_{ao}$ and $Fe_{bi}-Fe_{bo}$ is only 2.73 kcal/mol above **H-1(b)**$^-$. The direct conversion between **H-1(c)**$^-$ and **H-1(b)**$^-$ involves rotation of the ligands about the Fe with the hydride, which results in cleaving a bridging ligand (either H or CO). The transition state for this rotation is

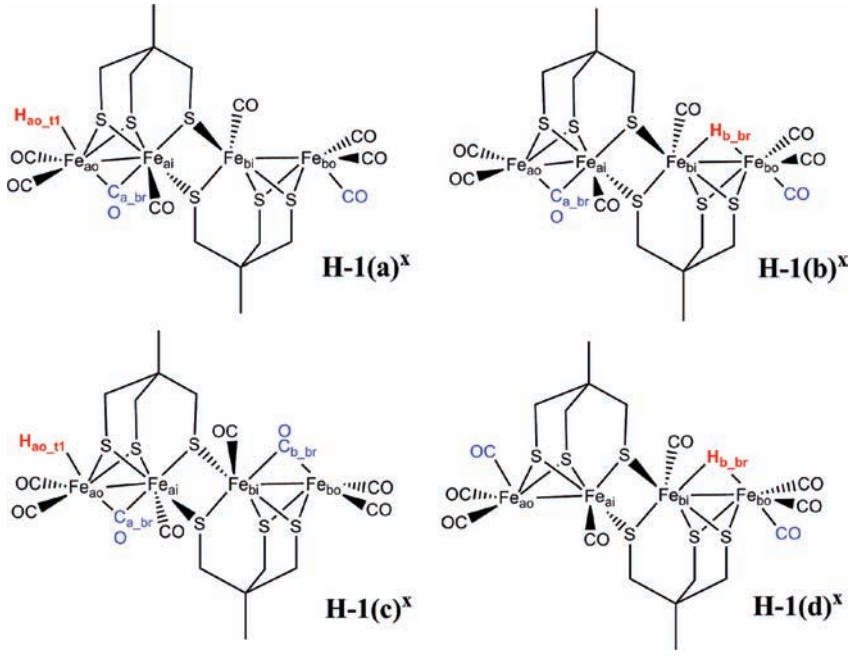

Figure 3. Possible structures of **H-1**^{x} (x = 2−, 1−, 0, and 1+) based on different arrangements of various hydride and CO ligands. **H-1(a)**^{x} has a terminal hydride on Fe_{ao}, a bridging CO between the $Fe_{ao}-Fe_{ai}$ bond, and all terminal COs on Fe_{bo}. **H-1(b)**^{x} has a bridging hydride between $Fe_{bo}-Fe_{bi}$ bond, all terminal COs on Fe_{bo}, and a bridging CO between the $Fe_{ao}-Fe_{ai}$ bond. **H-1(c)**^{x} has a terminal hydride on Fe_{ao} and a bridging CO between the $Fe_{ao}-Fe_{ai}$ bond and between the $Fe_{bo}-Fe_{bi}$ bond. **H-1(d)**^{x} has a bridging hydride between the $Fe_{bo}-Fe_{bi}$ bond and all terminal COs on both Fe_{ao} and Fe_{bo}.

Table 4. Solvation (CH_2Cl_2)-Corrected Relative Free Energies of **H-1**^{x} (x = 2−, 1−, 0, and 1+) with Respect to the Most Stable Structure

	1+	0	1−	2−
H-1(a)	15.01	9.47	7.34[c]	n/I[b]
H-1(b)	n/I[a]	10.78	0.00	5.20
H-1(c)	38.58	17.12[c]	2.73	0.00
H-1(d)	0.00	0.00	5.52[c]	n/I[d]

[a] The structure is found as **H-1(d)**$^+$. [b] The structure is found as **H-1(c)**$^{2-}$. [c] These structures are transition states. [d] The structure is found as **H-1(b)**$^{2-}$.

Table 5. Proton-Transfer Free Energies (ΔG^{PT}) of n**H-1**^{x} with CH_2Cl_2 Solvation Correction Calculated from the Reaction $LutH^+ + n\mathbf{H\text{-}1}^x \rightarrow Lut + (n+1)\mathbf{H\text{-}1}^{(x+1)}$ (n = 0, 1, and 2; x = 2−, 1−, and 0)

reaction	ΔG^{PT}
I + $LutH^+ \rightarrow$ **H-1(d)**$^+$ + Lut	21.46
1$^-$ + $LutH^+ \rightarrow$ **H-1(d)** + Lut	−6.25
1^{2-} + $LutH^+ \rightarrow$ **H-1(b)**$^-$ + Lut	−19.83
1^{2-} + $LutH^+ \rightarrow$ **H-1(c)**$^-$ + Lut	−17.10
H-1(d) + $LutH^+ \rightarrow$ **2H-1(e)**$^+$ + Lut	15.44
H-1(b)$^-$ + $LutH^+ \rightarrow$ **2H-1(d)** + Lut	−5.10
H-1(c)$^{2-}$ + $LutH^+ \rightarrow$ **2H-1(c)**$^-$ + Lut	−21.77
2H-1(e) + $LutH^+ \rightarrow$ **3H-1(d)**$^+$ + Lut	34.03
2H-1(d)$^-$ + $LutH^+ \rightarrow$ **3H-1(d)** + Lut	−10.26

29.5 kcal/mol above **H-1(b)**$^-$ (see SI for additional details). Thus, conversion between **H-1(c)**$^-$ and **H-1(b)**$^-$ should be slower than electron or proton transfer.

Like the cationic and neutral complexes, the lowest energy structure for the anions, **H-1(b)**$^-$, also has a bridging hydride between $Fe_{bi}-Fe_{bo}$, but it also has a bridging CO between $Fe_{ai}-Fe_{ao}$, instead of all terminal COs as found in **H-1(d)**$^+$ and **H-1(d)** (Figure 3). The proton-transfer free energy of **1**$^{2-}$ to form **H-1(b)**$^-$ is quite favorable at −19.83 kcal/mol (Table 5). Again in **H-1(b)**$^-$ the atomic charges of $Fe_{bo}-Fe_{bi}$, the pair with the bridging hydride, are more negative than those of $Fe_{ai}-Fe_{ao}$, the pair without the bridging hydride (Table 1), and the $Fe_{bi}-Fe_{bo}$ bond is longer than the $Fe_{ai}-Fe_{ao}$ bond by 0.08 Å (Table 2). The proton-transfer free energy of **1**$^{2-}$ to form **H-1(c)**$^-$ is also favorable at −17.10 kcal/mol. The Fe−Fe bond distances in **H-1(c)**$^-$ are not significantly different from those in **1**$^{2-}$ (Table 2). However, with a proton terminally bound at Fe_{ao}, the bridging CO in **H-1(c)**$^-$ shifts away from Fe_{ao} toward Fe_{ai}; the $Fe_{ao}-C_{a\_br}$ bond is lengthened (from 1.850 to 2.107 Å) and the $Fe_{ai}-C_{a\_br}$ bond is shortened (from 2.069 to 1.898 Å), a movement reflecting the strong hydride trans influence. The role of **H-1(b)**$^-$ and **H-1(c)**$^-$ species in the dihydrogen production will be discussed later.

The proton addition to **1**, **1**$^-$, and **1**$^{2-}$ forms **H-1**$^+$, **H-1**, and **H-1**$^-$, respectively, but reduction of **H-1**$^-$ can form the new species **H-1**$^{2-}$. Here, **H-1(a)**$^{2-}$ and **H-1(d)**$^{2-}$ cannot be located, as during their geometry optimizations, one of the CO ligands on the outer iron rotates from a terminal to a bridging position and these structures become **H-1(c)**$^{2-}$ and **H-1(b)**$^{2-}$, respectively (Figure 3). Although we did not confirm the nature of the **H-1(a)**$^{2-}$ and **H-1(d)**$^{2-}$ structures, we suspect that they are saddle points as in our previously confirmed cases. Unlike the monoanion, the dianion **H-1(c)**$^{2-}$, a terminal hydride complex, is more stable than **H-1(b)**$^{2-}$, a bridging hydride complex, by −5.20 kcal/mol (Table 4). This is another example of this system preferring bridging COs when the electron density available on the Fe atoms increases. In comparison to **H-1(c)**$^-$, the dianion **H-1(c)**$^{2-}$ has $Fe_{ao}-Fe_{ai}$ and $Fe_{ai}-Fe_{bi}$ bonds lengthened by 0.14 and 0.08 Å, respectively, and the outer iron atoms, Fe_{ao} and Fe_{bo}, become more electron rich (Table 1). Note that from the atomic charges, the hydride (H_{ao_t1}) in **H-1(c)**$^{2-}$ appears more hydridic than the hydride in **H-1(c)**$^-$ and would be expected to abstract another proton to form H_2 more easily (vide infra).

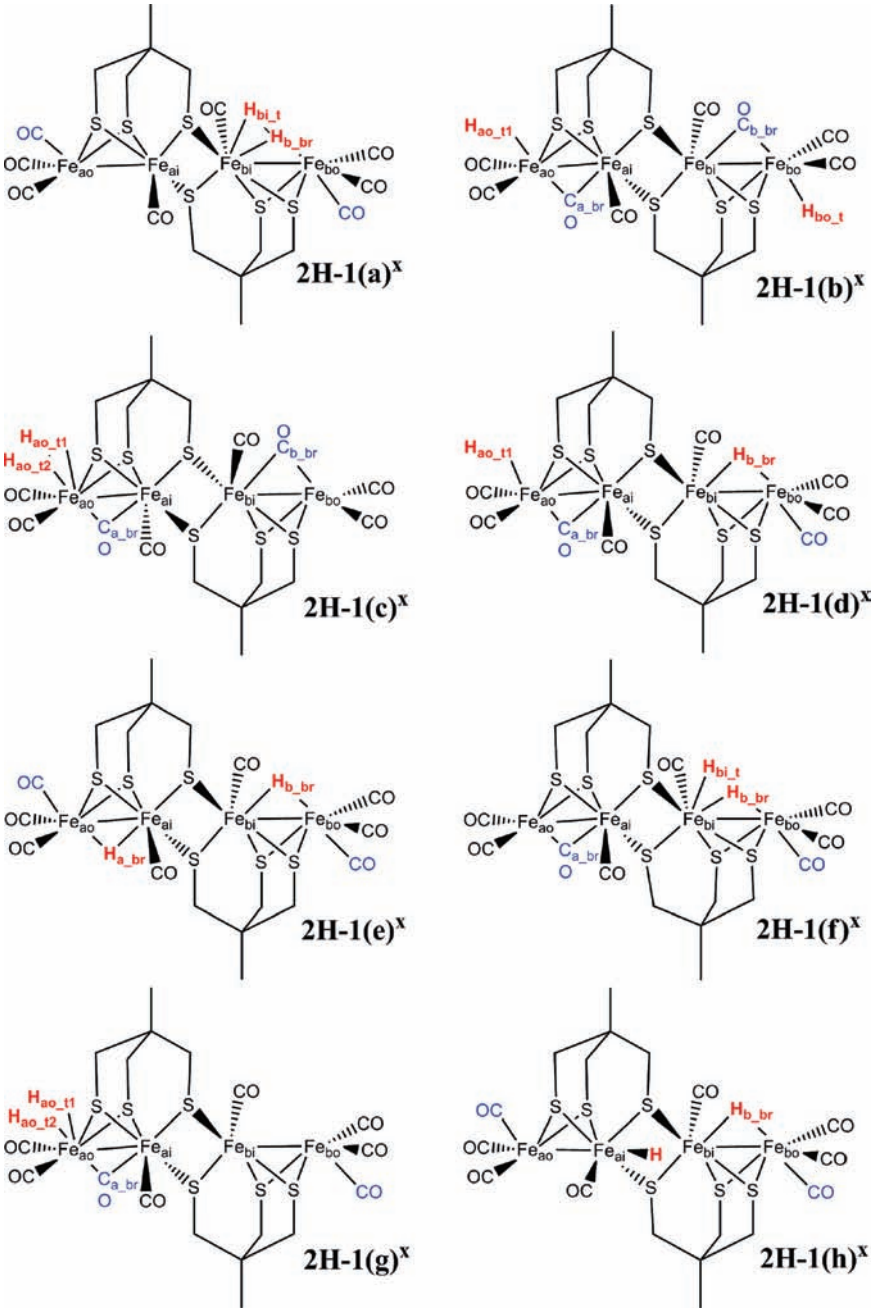

Figure 4. Possible structures of **2H-1**^{x} (x = 1−, 0, and 1+) based on different arrangements of hydrides and CO ligands.

3. Second Proton Addition: 2H-1$^+$, 2H-1, and 2H-1$^-$. Proton addition to **H-1**, **H-1**$^-$, and **H-1**$^{2-}$ forms **2H-1**$^+$, **2H-1**, and **2H-1**$^-$, respectively. As described above, the formation of **H-1**$^+$ is unlikely; therefore, **2H-1**$^{2+}$ structures were not examined. Possible structures of **2H-1**^{x} (x = 1−, 0, and 1+) are shown in Figure 4 based on the arrangements of two hydrides and CO ligands in the molecule; their relative energies are also shown in Table 6. Interestingly, the structure with bridging hydrides between Fe_{ai}−Fe_{ao} and Fe_{bi}−Fe_{bo} and all terminal COs on Fe_{ao} and Fe_{bo}, **2H-1(e)**^{x}, is the most stable structure in all cationic, neutral, and anionic **2H-1**^{x} species.

For the cations, **2H-1(e)**$^+$ is more stable than **2H-1(d)**$^+$, the structure with a hydride (H_{b_br}) bridging between the Fe_{bi}−Fe_{bo} bond, a terminal hydride (H_{ao_t1}) on Fe_{ao}, and a bridging carbonyl between the Fe_{ai}−Fe_{ao} bond (Figure 4), by 12.61 kcal/mol and more stable than other structures by 24−34 kcal/mol (Table 6). The proton-transfer free energy to **H-1(d)**, the lowest energy structure of **H-1**, to form **2H-1(e)**$^+$ is unfavorable by 15.44 kcal/mol (Table 5). Therefore, as for **H-1(d)**$^+$, the cationic species **2H-1(e)**$^+$ is unlikely to be formed in the reaction.

Among the neutral species, **2H-1(d)** lies close to **2H-1(e)**, the former higher in energy by 5.26 kcal/mol, whereas other structures have significantly higher energies than **2H-1(e)** by 11−30 kcal/mol. Proton transfer to **H-1(b)**$^-$ (Figure 3), the most stable structure of **H-1**$^-$, would initially lead (no structural rearrangement) to **2H-1(d)** (Figure 4) with −5.10 kcal/mol in proton transfer free energy (Table 5). Then, **2H-1(d)** could convert to **2H-1(e)**, the most stable structure, through the rotation of the bridging CO and terminal hydride. However, the transition state

Table 6. Solvation (CH_2Cl_2)-Corrected Relative Free Energies of **2H-1**^{x} (x = 1−, 0, and 1+) with Respect to the Most Stable Structure

	1+	0	1−
2H-1(a)	28.88	29.58	n/l[d]
2H-1(b)	26.17	11.53	5.60
2H-1(c)	33.93	n/l[a]	0.96
2H-1(d)	12.61	5.26	2.36
2H-1(e)	0.00	0.00	0.00
2H-1(f)	34.22	n/l[b]	7.63
2H-1(g)	24.08	n/l[c]	n/l[c]
2H-1(h)	n/c[e]	12.71	8.35

[a] The structure is found as **2H-1(g)**. [b] The structure is found as **2H-1(a)**. [c] The minimum structure is not found because H_2 dissociates from the Fe center. [d] The structure is found as **2H-1(f)**$^-$. [e] The structure is not calculated.

for this rotation would be expected to be ~25 kcal/mol on the basis of its similarity to the transition state between **H-1(c)**$^-$ and **H-1(b)**$^-$. Because of symmetry, the atomic charges in **2H-1(e)** are nearly equal for the Fe_{ai}−Fe_{ao} and the Fe_{bi}−Fe_{bo} pairs, with more negative charge on the outer Fe than on the inner Fe (Table 1). The **2H-1(e)** could be an intermediate for hydrogen production and regeneration of **1**, as the free energy for hydrogen production is favorable by −8.91 kcal/mol (Table 7). However, the positions of two hydrogen atoms in **2H-1(e)** are too far from each other to directly form a hydrogen molecule. To produce the hydrogen molecule, a bridging hydride on one of the inner−outer Fe pairs in **2H-1(e)** needs to move closer to the other hydride; the process could involve hydride transfer to the inner Fe closer to the other hydride through an intermediate like **2H-1(h)** (Figure 4), for which the energy is higher than **2H-1(e)** by 12.71 kcal/mol. Although the overall energy for the hydrogen production by **2H-1(e)** is exergonic, the reaction necessarily proceeds through a higher energy intermediate, such as **2H-1(h)**, and would be expected to have an even higher energy transition state (barrier) to reach this intermediate.

One might expect **2H-1(c)** (Figure 4) to be formed through the protonation of **H-1(c)**$^-$, which is only 2.73 kcal/mol less stable than **H-1(b)**$^-$ (Figure 3 and Table 4). However **2H-1(c)** could not be located as the bridging CO rotates to a terminal position, becoming **2H-1(g)** (Figure 4). Thus, **2H-1(c)** does not exist but is a transition state on the energy surface, and moreover, neither the dihydride- nor the dihydrogen-bound state of **2H-1(g)** could be found; instead, the two hydrogen atoms on the same outer Fe in **2H-1(g)** form a hydrogen molecule, which dissociates from the iron center during the geometry optimization. Thus, the hydride in **H-1(c)**$^-$ could abstract the proton from $LutH^+$, liberate H_2, and regenerate **1**, rapidly. The hydrogen production directly from **H-1(c)**$^-$ and $LutH^+$ is calculated to be favorable by −22.00 kcal/mol (Table 7).

For the dihydride anionic species, **2H-1(d)**$^-$ lies even closer to the lowest energy structure **2H-1(e)**$^-$ (2.36 kcal/mol) (Table 6). However, the hydrogen molecule cannot be produced directly from either **2H-1(e)**$^-$ or **2H-1(d)**$^-$ because the two hydrogen atoms are located at different sites in these molecules (Figure 4); therefore, the H_2 formation would have to proceed through higher energy transition states and intermediates, such as **2H-1(h)**$^-$ (8.35 kcal/mol relative to **2H-1(e)**$^-$). On the other hand, the structure with two hydrogen atoms in terminal positions on the same outer Fe (Fe_{ao}), **2H-1(c)**$^-$ (Figure 4), is only 0.96 kcal/mol higher energy than **2H-1(e)**$^-$ and can be formed readily through the proton transfer to **H-1(c)**$^{2-}$ (−21.77 kcal/mol) (Table 5). The **2H-1(c)**$^-$ can produce H_2 and regenerate **1**$^-$, releasing energy of −20.77 kcal/mol (Table 7).

Table 7. Free Energies for H_2 Releasing (ΔG^{H2}) of ***n*H-1**^{x} with CH_2Cl_2 Solvation Correction Calculated from the Reaction ***n*H-1**$^x \rightarrow H_2 + (n-2)$**H-1**^{x} ($n$ = 2 and 3; x = 1− and 0)

reaction	ΔG^{H2}
H-1(c)$^-$ + $LutH^+ \rightarrow$ **1** + Lut + H_2	−22.00
2H-1(e) $\rightarrow$ **1** + H_2	−8.91
2H-1(h) $\rightarrow$ **1** + H_2	−21.62
2H-1(c) $\rightarrow$ **1**$^-$ + H_2	−20.77
3H-1(d) $\rightarrow$ **H-1(d)** + H_2	−18.16

4. Third Proton Addition: 3H-1$^+$**, 3H-1, and 3H-1**$^-$**.** The third proton addition forms **3H-1**^{x} (x = 1−, 0, and 1+) in structures shown in Figure 5. The three hydrogen atoms in the **3H-1**^{x} optimized structures are located such that two hydrogen atoms are on the same di-iron subsite, whereas the third hydrogen atom is on the other di-iron subsite. The cationic species **3H-1**$^+$ is formed by the proton addition to **2H-1**. The lowest energy structure, **3H-1(d)**$^+$, has two terminal hydrides (H_{ao_t1} and H_{ao_t2}) at the same outer Fe (Fe_{ao}) and a bridging hydride (H_{b_br}) between Fe_{bi}−Fe_{bo}. The structure with a terminal hydride on Fe_{bi} (H_{bi_t}) and bridging hydrides between both Fe_{bi}−Fe_{bo} (H_{b_br}) and Fe_{ai}−Fe_{ao} (H_{a_br}), **3H-1(c)**$^+$ is 1.56 kcal/mol above **3H-1(d)**$^+$, while **3H-1(a)**$^+$ and **3H-1(b)**$^+$ have higher energies than **3H-1(d)**$^+$ by ~10 kcal/mol (Table 8). As in **H-1(d)**$^+$ and **2H-1(e)**$^+$, the cationic species **3H-1(d)**$^+$ is an unlikely intermediate in the reaction, as the proton-transfer free energy to **2H-1(e)** to form **3H-1(d)**$^+$ is endergonic by 34.04 kcal/mol (Table 5).

For the neutral species, **3H-1(d)** is still the lowest energy structure, more stable than **3H-1(c)** by −7.16 kcal/mol (Figure 5 and Table 8); once again, one expects that hydrogen production would be more favorable at a single Fe_{ao} in **3H-1(d)** rather than at the bridging Fe_{bi}−Fe_{bo} site in **3H-1(c)**. **3H-1(d)** can be formed by proton transfer to **2H-1(d)**$^-$, which is favorable by −10.26 kcal/mol (Table 5), and the production of H_2 from **3H-1(d)** regenerates **H-1(d)** exergonically by −18.16 kcal/mol (Table 7).

Reduction of neutral **3H-1** forms the anionic species **3H-1**$^-$. For this anion, the **3H-1(b)**$^-$ and **3H-1(d)**$^-$ structures, in which two terminal hydrogen atoms (H_{ao_t1} and H_{ao_t2}) are at the same outer iron (Fe_{ao}), could not be located because during the geometry optimization the two hydrogen atoms form a hydrogen molecule that dissociates from the iron center (Figure 5 and Table 8). On the other hand, structures with two hydrogen atoms posed to form a hydrogen molecule at the Fe_{bi}−Fe_{bo} site, **3H-1(a)**$^-$ and **3H-1(c)**$^-$, can be located as minima. **3H-1(c)**$^-$ is found more stable than **3H-1(a)**$^-$ by −3.47 kcal/mol, and it could release H_2 and regenerate **H-1(b)**$^-$ exergonically by −29.60 kcal/mol.

Among the **3H-1**^{x} species (x = +1, 0, and −1), when one compares the structures that have the same position of two hydrogen atoms at one iron pair, the third hydrogen atom prefers to be at the bridging position between the other inner−outer Fe−Fe bond rather than at the terminal position on the outer Fe; that is, **3H-1(d)**^{x} is more stable than **3H-1(b)**^{x} and **3H-1(c)**^{x} is more stable than **3H-1(a)**^{x} by a

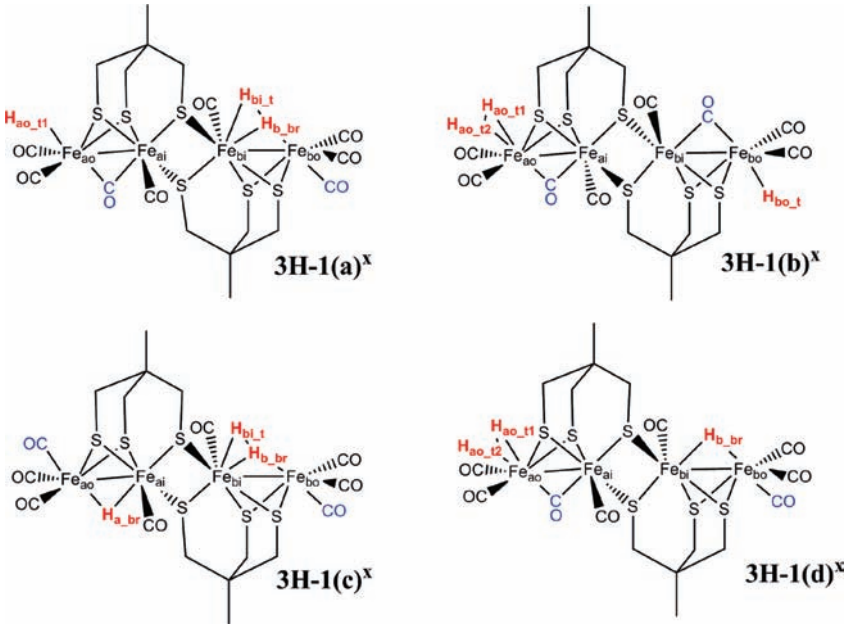

Figure 5. Possible structures of **3H-1**^{x} (x = 1−, 0, and 1+) based on different arrangements of hydrides and CO ligands.

Table 8. Solvation (CH_2Cl_2)-Corrected Relative Free Energies of **3H-1**^{x} (x = 1−, 0, and 1+) with Respect to the Most Stable Structure

	1+	0	1−
3H-1(a)	10.75	13.05	3.47
3H-1(b)	10.66	5.76	n/l[a]
3H-1(c)	1.56	7.16	0.00
3H-1(d)	0.00	0.00	n/l[a]

[a] The minimum structure is not found because H_2 dissociates from the Fe center.

similar amount of free energy (Table 8). This corresponds to the experimental observation for di-iron complexes that the bridging hydride structure is generally more stable and inert than the terminal hydride structure.[24,68]

5. Calculated Reduction Potential. The calculated reduction potentials of **1** and **1**$^-$ are −0.92 and −1.74 V (vs Fc/Fc^+) (Table 9), whereas the experimental values are −1.22 and −1.58 V, respectively (vs Fc/Fc^+).[43,44] Within the error of the calculated reduction potential (∼0.3 V), we can determine the possible intermediates formed at the first applied potential that initially reduces **1** to **1**$^-$ and at the lower (more negative) applied potential that initially reduces **1**$^-$ to **1**$^{2-}$. The spectroelectrochemical experiment[44] on **1** in the presence of $LutH^+$ acid showed that at the first applied potential, where **1** is reduced to **1**$^-$, the concentration of $LutH^+$ decreases very slowly with **1**$^-$ as a main species in solution. At the lower applied potential, where **1**$^-$ is reduced to **1**$^{2-}$, the concentration of $LutH^+$ decreases more rapidly. These observations are consistent with our calculation in the following ways.

Figure 6 summarizes the thermodynamic relationships among the key low-energy ***n*H-1**^{x} (n = 0, 1, 2, and 3; x = 2−, 1−, 0, and 1+) species along with the possible reaction paths in the hydrogen production by the tetra-iron hexa-thiolate complex $Fe_4[MeC(CH_2S)_3]_2(CO)_8$ (**1**). On the basis of the comparison of the measured and calculated E^0 compared

Table 9. Calculated Reduction Potential (E^0 vs Fc/Fc^+) with Solvation (CH_2Cl_2) Correction of Selected Structures of **H-1**^{x}, **2H-1**^{x}, and **3H-1**^{x} (x = 1−, 0, and 1+)

reaction	E^0 (V)
1 + e^- → **1**$^-$	−0.92
1$^-$ + e^- → **1**$^{2-}$	−1.74
H-1(d)$^+$ + e^- → **H-1(d)**	0.28
H-1(d) + e^- → **H-1(b)**$^-$	−1.15
H-1(b)$^-$ + e^- → **H-1(c)**$^{2-}$	−1.93
H-1(c)$^-$ + e^- → **H-1(c)**$^{2-}$	−1.81
2H-1(e)$^+$ + e^- → **2H-1(e)**	−0.03
2H-1(d) + e^- → **2H-1(d)**$^-$	−1.26
3H-1(d)$^+$ + e^- → **3H-1(d)**	0.43

above and in other work, we expect our calculated E^0 for $[X]^0$ reductions to $[X]^{1-}$ to appear too high, while those for $[X]^{1-}$ reductions to $[X]^{2-}$ to appear too low.

(1) At the first applied reduction potential, which reduces **1** to **1**$^-$, **1**$^-$ can be protonated by the acid $LutH^+$ at the inner−outer Fe−Fe bond to form **H-1(d)**, the most stable **H-1** species with a bridging hydride and all terminal CO ligands. At this potential the reduction of **H-1(d)** can then occur to form **H-1(b)**$^-$. Although one might expect **H-1(d)**$^-$, as it has a structure with all terminal COs like **H-1(d)**, **H-1(d)**$^-$ is a transition state, so it rapidly converts to the most stable structure, **H-1(b)**$^-$. The rearrangement of **H-1(b)**$^-$ to the higher energy isomer **H-1(c)**$^-$, which can directly react with $LutH^+$ and liberate H_2, needs to pass over a high barrier for the rotation of the bridging hydride and the terminal CO. Thus, **H-1(b)**$^-$ adds another proton terminally to the outer iron to form **2H-1(d)**; this species could rearrange to the more stable equilibrium form, **2H-1(e)**, with a bridging hydride on both inner−outer iron pairs and would pass over a similar high barrer to do so. Since all **2H-1** species are too acidic to be protonated to **3H-1**$^+$ species, most H_2 production must proceed from **2H-1** rearrangement. Although further reduction of **2H-1** species would open up

(68) Zhao, X.; Chiang, C. Y.; Miller, M. L.; Rampersad, M. V.; Darensbourg, M. Y. *J. Am. Chem. Soc.* **2003**, *125*, 518–524.

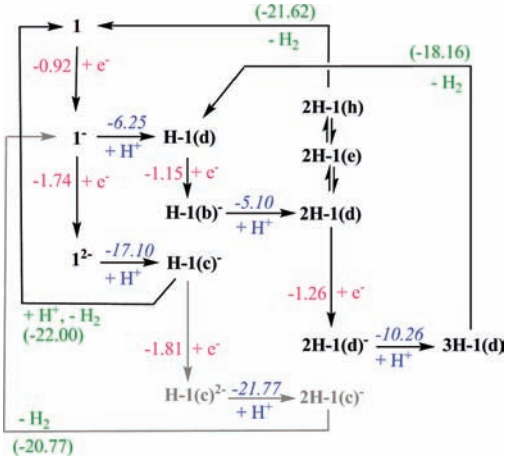

Figure 6. Thermodynamic relationships among ***n*H-1^x** (n = 0, 1, 2, and 3; x = 2−, 1−, 0, and 1+). The electron addition and calculated reduction potentials in V (vs Fc/Fc^+) are shown on the vertical arrow pointing down. The proton-transfer free energies in kcal/mol are shown on the horizontal arrow. The free energies for the H_2 releasing are shown in parentheses in kcal/mol.

an additional route to H_2 production routes, as shown in Figure 6, we believe that this potential is somewhat too low. Thus, from **2H-1(e)**, one of the bridging hydrides transfers to the inner iron to a position close to the other bridging hydride through the higher energy intermediate **2H-1(h)**; both this rearrangement and H_2 release from this species would have even higher energy transition states. Therefore, the rate of $LutH^+$ consumption at the first applied potential through this ECEC (electrochemical−chemical−electrochemical−chemical) process is quite low, as observed from the spectroelectrochemical experiment.

(2) At the lower applied potential $\mathbf{1}^-$ will be reduced further to $\mathbf{1}^{2-}$. Since $\mathbf{1}^{2-}$ has COs occupying the bridging sites, protonation occurs at a terminal site and **H-1(c)**$^-$ is produced, by the first proton transfer (Figures 2 and 3); **H-1(c)**$^-$ is a stable species only 2.73 kcal/mol higher energy than **H-1(b)**$^-$, and the transition state for the rearrangement is calculated to be high. Thus, **H-1(c)**$^-$ will add a second proton before it rearranges to **H-1(b)**$^-$; this second proton produces an unstable species that release H_2 and regenerates **1** directly (exergonic by −22.00 kcal/mol). Thus, at the lower applied reduction potential, the formation of **H-1(c)**$^-$ produces H_2 spontaneously without going through **2H-1(d)**, **2H-1(e)**, and other higher energy intermediates. This result corresponds to the experimental observation that at this lower applied reduction potential, the concentration of $LutH^+$ decreases rapidly with recovery of the neutral species, **1**, in an EECC process. Note that the faster rate of electron transfer at the lower reduction potential could also contribute to an increase in the overall rate at this potential. Further, **2H-1(d)**, which can be formed at the first applied potential, can now be reduced further to **2H-1(d)**$^-$ (−1.26 V), which could be protonated to **3H-1(d)**, which in turn would release H_2 (Figure 6). However, this hydrogen production path is expected to be a minor route at the potential that can transfer two electrons to **1**, as the concentrations of **H-1(d)** and **2H-1(d)** are expected to be lower than $\mathbf{1}^{2-}$ and **H-1(c)**$^-$. A small amount of unidentified intermediates observed in the experiment[44] may correspond to these and other related protonated species.

(3) Our calculated reduction potentials suggested that if an even lower reduction potential is applied, then other intermediates could be accessed for H_2 production, for example, reduction of **H-1(c)**$^-$ to form **H-1(c)**$^{2-}$, which is easily protonated to **2H-1(c)**$^-$. With two hydrogens binding terminally on the same outer iron, **2H-1(c)**$^-$ can generate directly H_2 and $\mathbf{1}^-$, exergonically, by −20.77 kcal/mol. Moreover, although the amount of **3H-1(d)** may be expected to be small, the reduction of **3H-1(d)** could lead to the H_2 production spontaneously as the hydrogen-bound state of **3H-1(d)**$^-$ is not located and H_2 dissociates from the iron center during the geometry optimization.

Conclusions

Direct calculations of reduction potentials and relative acidities by density functional theory of species derived from the iron complex $Fe_4[MeC(CH_2S)_3]_2(CO)_8$ show the most probable routes: (1) at the first (less negative) reduction potential H_2 is produced slowly through an ECEC route and (2) at the second (more negative) potential H_2 is produced more rapidly through an EECC route. These direct predictions agree with conclusions based on the experimental work.[44] Although both routes arrive at a doubly reduced, singly protonated species in the third step of these processes, these related species are different. After the ECE step in the slower route, the species has a bridging H, while after the EEC step on the faster route, the species has a terminal H. The calculations predict that a high barrier prevents the rapid interconversion of these two nearly isoenergetic species. In the slower ECEC route, the second proton likely arrives at a site remote from the first and the species produced must pass over a significant energy barrier to produce H_2, while in the faster EECC route, the second proton likely arrives close to the first and the species produced rapidly releases H_2. Generally, it appears that terminal hydride structures become more favorable in more highly reduced species and that the rapid hydrogen production from reduction of **1** to $\mathbf{1}^{2-}$ is mainly through the proton reduction at a terminal position on a single iron rather than at a bridging position that is blocked by bridging COs in $\mathbf{1}^{2-}$. This conclusion lends further support to the notion that the protein structure in the [FeFe]-hydrogenase supports and maintains a bridging or semibridging CO and an open terminal site for protonation.

Acknowledgment. We would like to thank the National Science Foundation (Grant Nos. CHE-0518074, CHE-0541587, and CHE-0910552), The Welch Foundation (Grant No. A-0648), and Royal Thai Government for financial support.

Supporting Information Available: Frontier molecular orbitals of **1**, $\mathbf{1}^-$, and $\mathbf{1}^{2-}$ and absolute energies of related molecules. This material is available free of charge via the Internet at http://pubs.acs.org.